JACS
JOURNAL OF THE AMERICAN CHEMICAL SOCIETY

ARTICLE

pubs.acs.org/JACS

Perturbations of Aromatic Amino Acids Are Associated with Iron Cluster Assembly in Ribonucleotide Reductase

Adam R. Offenbacher, Jun Chen,[†] and Bridgette A. Barry*

Department of Chemistry and Biochemistry and the Petit Institute for Bioengineering and Bioscience, Georgia Institute of Technology, Atlanta, Georgia 30332, United States

Supporting Information

ABSTRACT: The β2 subunit of class Ia ribonucleotide reductases (RNR) contains an antiferromagnetically coupled μ-oxo bridged diiron cluster and a tyrosyl radical (Y122•). In this study, an ultraviolet resonance Raman (UVRR) difference technique describes the structural changes induced by the assembly of the iron cluster and by the reduction of the tyrosyl radical. Spectral contributions from aromatic amino acids are observed through UV resonance enhancement at 229 nm. Vibrational bands are assigned by comparison to histidine, phenylalanine, tyrosine, tryptophan, and 3-methylindole model compound data and by isotopic labeling of histidine in the β2 subunit. Reduction of the tyrosyl radical reveals Y122• Raman bands at 1499 and 1556 cm^{-1} and Y122 Raman bands at 1170, 1199, and 1608 cm^{-1}. There is little perturbation of other aromatic amino acids when Y122• is reduced. Assembly of the iron cluster is shown to be accompanied by deprotonation of histidine. A p^2H titration study supports the assignment of an elevated pK for the histidine. In addition, structural perturbations of tyrosine and tryptophan are detected. For tryptophan, comparison to model compound data suggests an increase in hydrogen bonding and a change in conformation when the iron cluster is removed. pH and ^2H_2O studies imply that the perturbed tryptophan is in a low dielectric environment that is close to the metal center and protected from solvent exchange. Tyrosine contributions are attributed to a conformational or hydrogen-bonding change. In summary, our work shows that electrostatic and conformational perturbations of aromatic amino acids are associated with metal cluster assembly in RNR. These conformational changes may contribute to the allosteric effects, which regulate metal binding.

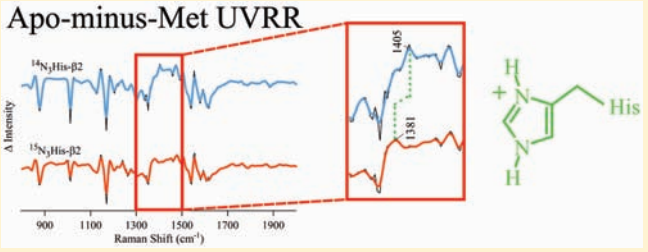

Ribonucleotide reductase (RNR) participates in DNA biosynthesis by reducing ribonucleotides to produce deoxyribonucleotides.[1] In all organisms, production of a transient cysteine radical at the active site is required for catalysis.[2] In *Escherichia coli* and other class Ia enzymes, RNR consists of two subunits, α2 and β2. The active site is located in the homodimeric α2 (formerly R1) subunit. The thiyl radical in α2 is generated by the stable tyrosyl radical (Y122•), which is adjacent to a diferric cofactor in the homodimeric β2 (formerly R2) subunit.[3] Reduction of Y122• and subsequent oxidation of C439 is proposed to be mediated by reversible long-distance proton-coupled electron transfer (PCET) reactions. These reactions occur over a conserved pathway and a distance of 35 Å.[4,5]

The catalytically essential Y122• forms during the activation of the apoprotein (Apo-β2).[6] The apoprotein lacks both the iron cluster and the tyrosyl radical, but these species are spontaneously generated in the presence of Fe^{2+} and molecular oxygen.[7] During the reduction of O_2, two reducing equivalents are provided by the oxidation of the iron cluster and a third originates from the oxidation of Y122. The fourth electron most likely arises from exogenous reductant(s).[6,7] The mechanism of β2 activation is an important process in class I RNR chemistry and is not yet fully understood (reviewed in ref 8).

The crystal structures of Apo-β2 (Figure 1B),[9] Red-β2 (diferrous protein),[10] and Met-β2 (Figure 1A; diferric protein lacking the tyrosyl radical)[11,12] have been solved. In comparison of these structures, no significant global structural changes were observed, apart from the local perturbations surrounding the diiron cluster. Furthermore, removal of the iron was inferred to cause protonation of ligating histidine residues.[9] Such protonation would provide charge compensation for a cluster of formerly ligating carboxylate groups. Local rearrangements of amino acid side chains in the vicinity of the metal site were also observed. Most notably, rotameric shifts in the conformation of aspartate and glutamate residues were evident when the Met-β2 and Apo-β2 structures were compared (Figure 1A,B).

Protein dynamics are proposed to play an important role in RNR. Although there is no three-dimensional structure of the fully oxidized, active protein, electron paramagnetic resonance (EPR)[12] and Fourier-transform infrared (FT-IR)[13] spectroscopic studies have given insight into the structural changes linked with Y122 redox changes. Reduction of the tyrosyl radical with hydroxyurea was observed to perturb the structure of the amide bond[13] and result in rotation of Y122.[12] In addition,

Received: September 11, 2010
Published: April 12, 2011

dx.doi.org/10.1021/ja107918g | *J. Am. Chem. Soc.* 2011, 133, 6978–6988

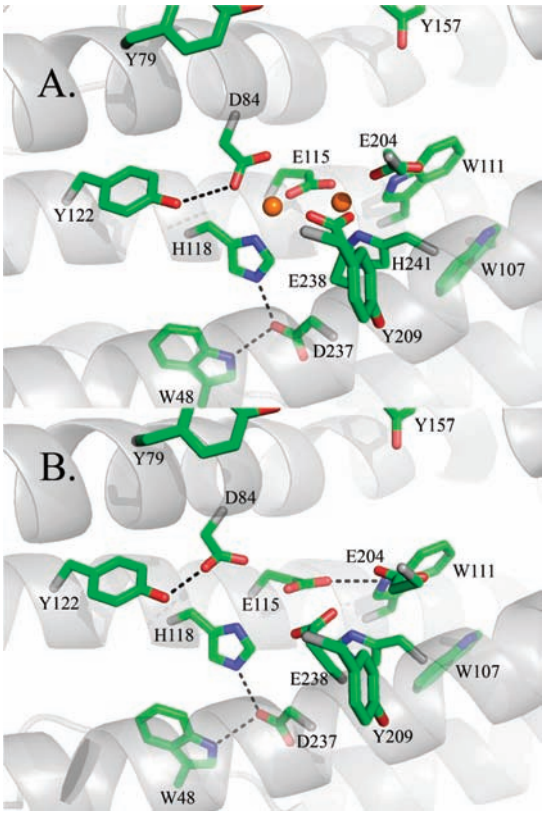

Figure 1. (A) The coordination environment of the Met-β2 *E. coli* subunit, which contains a diferric cluster and a reduced tyrosyl radical (PDB ID: 1RIB). All histidine, tryptophan, and tyrosine residues located within 11 Å of the cluster are shown. The iron atoms are displayed as orange spheres. The black, dashed lines represent hydrogen-bonding interactions discussed within the text. (B) The corresponding environment in the metal free (Apo-β2) *E. coli* β2 subunit (PDB coordinates were graciously provided by H. Eklund).

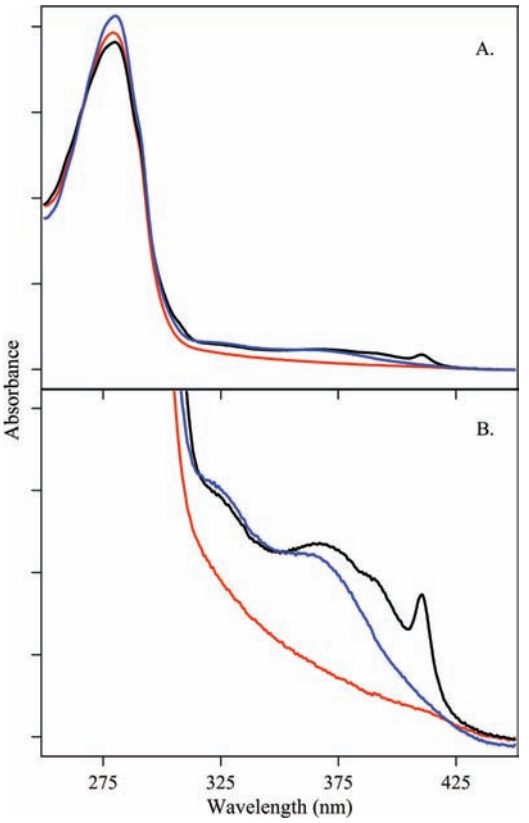

Figure 2. Room temperature UV−visible absorbance spectra of *E. coli* β2 samples. In both panels, the black line represents control β2, the blue line represents Met-β2, and the red line represents Apo-β2. The samples were prepared at 7.5 μM in 5 mM HEPES-NaOL, p^{1}H 7.6. The spectra in panel B were multiplied by a factor of 10. The *y*-axis tick marks represent 2.5 $\times$ 10^{-1} absorbance units.

carboxylate shifts occur during redox changes at the diiron cluster.[10] A slow protein conformational change has been proposed to be rate-limiting in enzymatic turnover.[14] A protein conformational change has also been proposed to accompany and possibly regulate the assembly of the diferric cluster in RNR.[15−17]

In this study, we employed ultraviolet resonance Raman (UVRR) spectroscopy to identify structural changes associated with the assembly of the iron cluster and with the reduction of the tyrosyl radical. Use of UV probe wavelengths enhances spectral contributions from histidine, tyrosine, and tryptophan side chains and allows structural changes in aromatic amino acids to be directly monitored (see ref 18 and the review in ref 19). The resonance Raman vibrational spectrum is sensitive to changes in protonation state, hydrogen bonding, and electrostatics. Difference UVRR spectroscopy allows a focus on the structural changes coupled with diferric cluster formation. Our data provide the first spectroscopic evidence for histidine protonation upon iron removal. With metal cluster assembly, significant differences are also induced in the structure and/or local environment of tyrosine and tryptophan residues. These experiments give new information concerning conformational changes that are coupled with metal binding in RNR.

EXPERIMENTAL SECTION

Materials. L-Tyrosine, L-tryptophan, L-histidine, L-phenylalanine, succinic acid, 4-(2-hydroxyethyl)piperazine-1-ethanesulfonic acid (HEPES), boric acid, lithium hydroxide, 8-hydroxyquinoline-5-sulfonic acid, 3-methylindole, cyclohexane, sodium hydroxide, hydrochloric acid, and hexamethylphosphoramide (HMPA) were obtained from Sigma (St. Louis, MO). Deuterium oxide, ^2H_2O (98%), and $^{15}N_3$-L-histidine:HCl:H_2O (98%) were purchased from Cambridge Isotope Laboratories (Andover, MA). Hydroxyurea was obtained from Calbiochem (San Diego, CA). Chloroform was purchased from J. T. Baker (Phillipsburg, NJ), and methanol was purchased from EMD (Gibbstown, NJ). NaOL refers to NaO^{1}H (Fisher Scientific, Pittsburg, PA) or NaO^{2}H (99.5%, Cambridge Isotopes).

***E. coli* β2 Overexpression, Purification, and ^{15}N Histidine Labeling.** *E. coli* wild-type (Wt) β2 protein was overexpressed and purified (Figure 2, black line) from *E. coli* BL21(DE3) cells transformed with pTB2, using protocols previously described.[13] The resulting yield was 60−120 mg of protein per liter. In this paper, the term, "control," will be used to refer to this isolated form of the β2 subunit, which contains both the tyrosyl radical and diferric cluster. Met-β2, the form of the protein lacking the tyrosyl radical but with an oxidized diiron cluster (Figure 2, blue line), was prepared by incubating with and subsequently removing hydroxyurea as described.[13] The iron-free form of the protein (Apo-β2; Figure 2, red line) was generated by dialyzing Met-β2 (2 mL, 100 μM) against an iron chelator, lithium 8-hydroxyquinoline-6-sulfonate (400 mL, 50 mM), as described.[7,20] The chelator was removed by

dialysis against 50 mM tris(hydroxymethyl)aminomethane (Tris)-HCl, 5% glycerol, pH 7.6, and subsequent chromatography on a desalting Sephadex G25 column. The ferrozine method of iron quantitation showed that at least 92% of the iron was removed by this treatment in the natural abundance sample. All protein samples were exchanged into 5 mM HEPES-NaOL, pL 7.6, through four sequential concentration and dilution steps using an Amicon (Beverly, MA) YM30 concentrator. The p^2H is reported as the uncorrected meter reading.[21]

^{15}N-histidine labeling was accomplished by overexpressing and purifying β2 from the histidine auxotroph, AW608Thr(DE3)/pTB2. *E. coli* AW608Thr cells were lysogenized with λDE3 using a kit from Novagen (Madison, WI) to incorporate the T7 gene. The minimal media used for incorporation of $^{15}N_3$-histidine was the same as described previously,[22] except 135 mg/L of labeled histidine was supplemented. The resulting yield was about 50 mg of protein per liter. Using this method, incorporation of ^{15}N into histidine has been confirmed previously by NMR spectroscopy.[23]

UV−Visible Absorption Spectroscopy. Absorption spectra of the purified *E. coli* β2 protein were collected at room temperature on a Hitachi U-3000 spectrophotometer in 1 cm quartz cuvettes. The scan settings were 120 nm min^{-1} and 2 nm slit width. The concentrations of the control, Met-β2, and Apo-β2 forms (Figure 2A) were determined using the $A_{280\ nm}$ and extinction coefficients of 131, 131, and 120 $mM^{-1}\ cm^{-1}$, respectively. The Y• yield for the control β2 protein was determined as previously described.[13] In the natural abundance preparation, quantitation yielded 1.1−1.4 Y• per dimer. In the $^{15}N_3$-histidine preparations, quantitation yielded 1.2 Y• per dimer.

UV Raman Experiments. UVRR spectra at 229 nm were recorded at room temperature using a Raman microscope system (Renishaw inVia, Hoffman Estates, IL) and 8 cm^{-1} spectral resolution.[24] The 250 μW, 229 nm probe beam was generated from a frequency-doubled Ar ion laser (Cambridge LEXEL 95, Fremont, CA). Samples were recirculated through a jet nozzle with a ~0.12 mm diameter to prevent UV damage. Control experiments at 400 μW UV probe power showed no significant alterations in the UVRR difference spectrum, Apo-β2 − Met-β2, supporting the conclusion that the samples were undamaged by the lower power, 250 μW UV probe beam. Protein samples were prepared at 50 μM concentrations and were exchanged into the appropriate buffer (usually 5 mM HEPES-NaOL, pL 7.6) prior to UVRR measurements. The exposure time was 21 min. To generate Raman difference spectra, UVRR data, recorded on the same day, were subtracted and averaged. Before subtraction, both spectra were corrected for any background and concentration fluctuation. The correction factor was generated by fitting a polynomial function to a background, which was generated by division of the two spectra. In this correction, the signal of water was adopted as an internal intensity standard.

Amino acid samples were prepared at 1 mM (tyrosine and tryptophan) or 20 mM (histidine and phenylalanine) concentrations in 5 mM HEPES-NaOL (pL 7.5; Y, W, F, H), borate-NaOL (pL 11.0; Y, H), or succinate-NaOL (pL 4.0; H). Spectra were acquired with a 250 μW, 229 nm probe beam and a 21 min exposure time. Solutions of 2 mM 3-methylindole were made in cyclohexane or cyclohexane plus 0.08% hexamethylphosphoramide (HPMA). Data were acquired with a 250 μW, 229 nm probe beam and a 3 min exposure time. To give the final spectrum, seven data sets were added. Difference spectra, showing the effects of changes in hydrogen bonding on 3-methylindole, were constructed by the method described above after subtraction of the solvent.

RESULTS

UV−Visible Absorption Spectra of β2. In Figure 2, we present the UV−visible absorption spectra of control, Met-β2, and Apo-β2 samples, which are similar to previous reports (for example, see ref 7). These data verify that metal extraction (Apo-β2) and tyrosyl radical reduction (Met-β2) have occurred. The control β2 absorbance spectrum (Figure 2A,B, black line) is defined by characteristic peaks at 325, 370, 390, and 410 nm. The μ-oxo bridged iron cluster contributes to the shoulder at 325 nm and the band at 370 nm.[7,25,26] The tyrosyl radical (Y122•) displays a characteristic sharp 410 nm band with a weak, broad 390 nm shoulder.[26] The Met-β2 state of the protein lacks the stable tyrosyl radical and therefore does not exhibit the 410 nm band (Figure 2A,B, blue line). When iron is removed, there is complete loss of spectral features >300 nm, as expected for Apo-β2 (Figure 2A,B, red line).

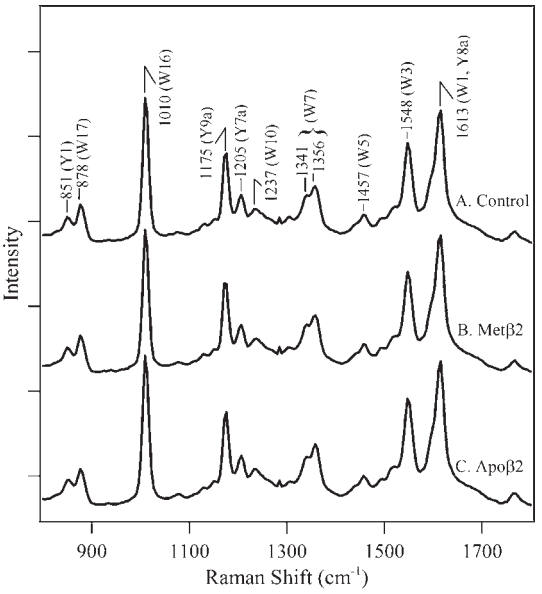

Figure 3. UVRR spectra of *E. coli* β2 collected with a 250 μW, 229 nm probe beam for a 21 min exposure time. The data were collected from control (A), Met-β2 (B), and Apo-β2 (C) samples. The protein concentrations were 50 μM in 5 mM HEPES-NaOL, p^1H 7.6. The spectra are representative data recorded from one sample. The *y*-axis tick marks represent 1×10^4 intensity units.

UVRR Spectra of β2. In Figure 3, we present the UVRR spectra of the control (Figure 3A), Met-β2 (Figure 3B), and Apo-β2 (Figure 3C) samples. The spectra were acquired with 229 nm excitation and at room temperature on a flowing sample. Overall, the UVRR spectra of the control, Met-β2, and Apo-β2 forms are similar (Figure 3). With 229 nm excitation, the vibrational bands of tryptophan and tyrosine are expected to be resonantly enhanced due to the overlap of the Raman probe with the B_b and L_a electronic transitions,[27,28] respectively. Histidine and phenylalanine have weaker Raman signals at this excitation wavelength due to their $\pi_1-\pi_1^*$ (histidine) and L_a (phenylanine) electronic transitions at ~207 nm.[27,29] To investigate the origin of the observed frequencies in the β2 subunit spectra (Figure 3), model compound UVRR data were acquired from tyrosine (Supporting Information, Figure S1), tryptophan (Supporting Information, Figure S2), phenylalanine (Supporting Information, Figure S3), and histidine (Supporting Information, Figure S4). See Figures and Table S1 in Supporting Information for a discussion of model compound assignments. On the basis of the model compound data, we conclude that the UVRR spectra of the β2 samples (Figure 3) are dominated by vibrational modes from tyrosine and tryptophan.

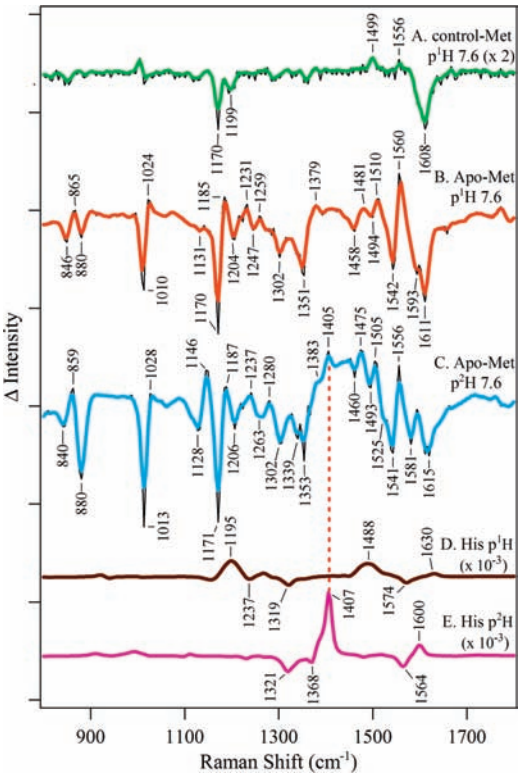

Figure 4. UVRR difference spectra of *E. coli* β2 samples. The data are control − Met-β2 in 5 mM HEPES-NaOL, p^{1}H 7.6 (A), Apo-β2 − Met-β2 in 5 mM HEPES-NaOL, p^{1}H 7.6 (B), Apo-β2 − Met-β2 in 5 mM HEPES-NaOL, p^{2}H 7.6 (C). In (D and E) are the protonation spectra of histidine in ^1H_2O and ^2H_2O, respectively, which correspond to subtractions of p^{1}H 4 − p^{1}H 7.5 and p^{2}H 4 − p^{2}H 7.5 in Figure S4 (Supporting Information). The spectrum in A was multiplied by 2 and the spectra in D and E have been multiplied by 10^{-3} for comparison. The green, orange, and light blue lines correspond to a three adjacent point smoothing fit to the raw (thin black line) data.[71] The spectra are averages of data obtained from (A) 10, (B) 10, (C) 10, (D) 3, and (E) 3 samples. The protein concentrations were 50 μM, and the histidine concentration was 20 mM. The *y*-axis tick marks represent 1×10^3 intensity units. See Table S1 in the Supporting Information for assignments.

UVRR Difference Spectra. In Figure 4, we present difference UVRR spectra for the control, Met-β2, and Apo-β2 samples. The difference spectra were constructed by subtraction of data, recorded on the same day and using an internal standard, as described in the Experimental Section. In these difference spectra, observed spectral features correspond to vibrational bands that are perturbed by tyrosyl radical reduction (Met-β2 samples) (Figure 4A) or by iron cluster removal (Apo-β2 samples) (Figure 4B,C). Use of difference spectroscopy focuses on spectral perturbations induced by reduction of the radical or by iron cluster assembly, respectively. Data in Figure 4A,B were acquired in ^1H_2O buffer; data in Figure 4C were acquired in ^2H_2O buffer. Figure 4 presents model compound difference spectra, constructed from data associated with the protonation of histidine in ^1H_2O (Figure 4D) or ^2H_2O (Figure 4E) buffers. These difference spectra were constructed by a direct one to one subtraction of the data in Figure S4 of the Supporting Information.

Spectral Changes Induced by Y122• Reduction, Relative to a Control Sample. In the control − Met-β2 difference spectrum (Figure 4A), unique Y122• contributions are positive bands, while unique Y122 contributions are negative bands. Oxidation of the tyrosine is expected to perturb CO stretching and aromatic ring stretching vibrations.[30−32] Both tyrosine and tyrosyl radical are resonantly enhanced with 229 nm excitation, because tyrosyl radical reduction shifts the L_a electronic transition from ~240 to 220 nm.[33] A previous UV Raman study of the tyrosyl radical in vitro assigned the Y7a CO stretching mode at 1510 cm^{-1} and the Y8a ring stretching mode at 1565 cm^{-1}.[31] A previous infrared study of the tyrosyl radical in vitro assigned the Y7a CO stretching mode at 1516 cm^{-1} and the Y8a ring stretching mode at 1554 cm^{-1}.[32,34]

In Figure 4A, the positive 1499 cm^{-1} feature is attributed to the Y7a mode of Y122•. This assignment is supported by previous visible Raman[35] and FT-IR[13] studies of RNR. In the FT-IR study, isotopic labeling of tyrosine was used to assign the Y7a band.[13] The 1499 cm^{-1} frequency is significantly downshifted compared to the CO frequency observed in model compounds and is upshifted from some of the reported frequencies for the photosystem II tyrosyl radicals.[36,37] Therefore, this CO frequency is diagnostic for the production of Y122•. In Figure 4A, a weak positive band at 1556 cm^{-1} is assigned to the ring stretching (Y8a) vibration of Y122•.[32,34]

The control − Met-β2 difference spectrum (Figure 4A) also exhibits negative bands at 1608, 1199, and 1170 cm^{-1}, which we attribute to the reduced tyrosine, Y122. The 1608 cm^{-1} band is assigned to the Y8a mode. While tryptophan (W1 at 1618 cm^{-1}) and phenylalanine (F8a at 1603 cm^{-1}) may make a contribution at 1608 cm^{-1}, phenylalanine has minimal resonance enhancement,[38] and the tryptophan W1 band is also weak with 229 nm Raman excitation. Y122 is protonated in the reduced state and either hydrogen bonded weakly to D84[12] or not hydrogen bonded.[11] The observed 1608 cm^{-1} frequency is between the frequency expected for a protonated (1614 cm^{-1}) and a deprotonated (1606 cm^{-1}) tyrosine. The Y8a and Y8b modes of tyrosine are not strongly influenced by hydrogen bonding.[39] However, the frequency of this band may be influenced by Stark effects, induced by the presence of the metal cluster.[40] The Y8b asymmetric mode (~1600 cm^{-1}; Supporting Information, Figure S1A, inset) overlaps with the Y8a band and is thus not resolvable in Figure 4A.

In Figure 4A, we assign the negative 1199 and 1170 cm^{-1} bands to tyrosine C_{ring}−CH_2− (Y7a) and CH bending (Y9a) deformation modes of Y122, respectively. The 1199 cm^{-1} band is expected to be sensitive to hydrogen bonding. The 1170 cm^{-1} band is expected to be sensitive to conformation. The Y7a C_{ring}−CH_2− stretch of tyrosine acts as a hydrogen-bond sensor in proteins, because the mode has a ∂COH component. For model tyrosine in solution, this band is observed at ~1210 cm^{-1} in non-hydrogen bonding or in proton-accepting, hydrogen-bonded tyrosine. This band is observed at ~1205 cm^{-1} in proton-donating, hydrogen-bonded tyrosine.[39] In Figure 4A, this band is observed at 1199 cm^{-1}, suggesting that the Y122 forms a hydrogen bond in the Met-β2 state. This observation is consistent with the high-resolution X-ray structure[12] (but see ref 11). The Y9a frequency for a protonated tyrosine is expected at approximately 1179 cm^{-1} (Supporting Information, Figure S1). Frequency shifts are not related to hydrogen bonding, but Y9a may downshift to 1170 cm^{-1} as the Y−OH hydrogen swings to an out-of-plane configuration.[39] An out-of-plane configuration is consistent with the X-ray structure of Met-β2 that assigns Y122 and D84 as hydrogen-bonding partners.[12]

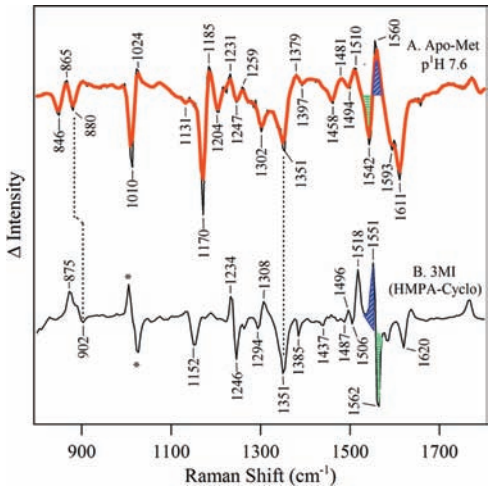

Figure 5. UVRR difference spectra of *E. coli* β2 and 3-methylindole model samples. The data in part A are Apo-β2 − Met-β2 in 5 mM HEPES-NaOL, p^{1}H 7.6. In part B, the 3-methylindole difference spectrum shows the effects of addition of 0.08% HPMA to cyclohexane (HPMA − no HPMA). The data in part A are reproduced from Figure 4B, for comparison. The orange line corresponds to a three adjacent point smoothing fit to the raw (thin black line) data.[71] The spectra are averages of data obtained from (A) 10 and (B) 7 samples. The protein concentration was 50 μM, and the 3-methylindole concentration was 2 mM. The asterisk in B corresponds to bands to which HPMA makes a contribution. The *y*-axis scale is arbitrary, to facilitate comparison of the spectra. See Experimental Section for details.

The intensity of the Y9a tyrosine feature band at 1175 cm^{-1} is approximately 10 000 counts in the control β2 UVRR spectrum (Figure 3A). The vibrational mode is unique to the tyrosine singlet state, because there is no associated positive spectral feature. The signal shown in Figure 4A is multiplied by 2 for comparison purposes. After correction for this, the intensity of the Y9a band in the control − Met-β2 difference spectrum (Figure 4A) is approximately 320 counts. Because there are 32 tyrosine residues in the β2 dimer,[41] we conclude that ~1 tyrosine residue contributes to the control − Met-β2 difference spectrum in Figure 4A. This result is consistent with an assignment of this band to Y122. Our UV−vis spectrophotometric characterization of the natural abundance β2 preparation gave a yield of 1.1−1.4 Y• per dimer. This experiment supports the conclusion that difference UV Raman spectroscopy monitors redox changes at Y122 in the β2 subunit. The spectrum is dominated by the bands associated with tyrosyl radical reduction, with little perturbation to other aromatic amino acid residues.

Spectral Changes Induced by Iron Cluster Removal, Relative to a Met-β2 Sample: Perturbations of Tryptophan. The Apo-β2 − Met-β2 difference spectrum (Figure 4B) displays spectral alterations due to iron cluster assembly. No significant contribution from Y122• reduction will be observed, because the tyrosyl radical is reduced under both sets of conditions. In Figure 4C, we present the Apo-β2 − Met-β2 difference spectra acquired in ^2H_2O buffer. As expected, significant differences are observed when compared to the control − Met-β2 data (Figure 4A). To promote exchange in Figure 4C, samples were incubated for >2 h in ^2H_2O buffer. Changing the length of the incubation from 2 to 36 h did not change the difference spectrum (data not shown). Assignments are summarized in Table S1 of the Supporting Information.

Comparison of the model compound data in Figures S1−S4 (Supporting Information) to Figure 4B supports the assignment of bands at 1010 (−)/1024 (+) cm^{-1} to the W16 mode of tryptophan (Figure 4B and Supporting Information, Table S1). Negative bands at 1351 (−), 1542 (−), and 1611 (−) cm^{-1} in Figure 4B are also assignable to tryptophan, with possible overlapping contributions from tyrosine for the 1611 cm^{-1} band. In Figure 4C, bands at 1128 (−) and 1146 (+) cm^{-1} are attributed to ^{2}H-exchanged tryptophan, based on comparison to the model compound spectra in ^2H_2O (Supporting Information, Figure S2).

A complex feature, 846 (−)/865 (+)/880 (−) cm^{-1}, is observed in the Apo-β2 − Met-β2 difference spectrum (Figure 4B). In model compound data, tyrosine has a spectral contribution at 849 cm^{-1} (Supporting Information, Figure S1), while tryptophan has a spectral contribution at 880 cm^{-1} (W17, Supporting Information, Figure S2). Therefore, this region may reflect overlapping contributions both from tyrosine (846 cm^{-1}) and tryptophan (880 cm^{-1}). The 880 cm^{-1} W17 tryptophan Raman band is expected to downshift ~20 cm^{-1} with ^{2}H exchange.[42] In agreement, our model compound results on tryptophan (Supporting Information, Figure S2) show an 18 cm^{-1} downshift on exchange. However, there is no shift for the W17 band in the Apo-β2 − Met-β2 difference spectrum (Figure 4C). This result implies that the ^{2}H exchange rate of the perturbed tryptophan is slow.[43]

To investigate the dependence of the UV Raman spectrum of tryptophan on hydrogen bonding and dielectric constant (ε), we conducted experiments on the model compound 3-methylindole (3MI) in cyclohexane (ε = 2.0) and cyclohexane plus 0.08% HPMA (Figure 5B).[44] HPMA forms strong hydrogen bonds as a proton acceptor and has been used to investigate the effects of hydrogen bonding on 3-methylindole previously.[45] Difference spectra, associated with an increase in hydrogen bonding, were constructed by the method employed for the protein data. This method corrects for any overall changes in Raman scattering intensity. As shown in Figure 5B, the model indole spectra are dominated by negative bands, as observed for the RNR data (Figure 5A). Marker bands for hydrogen bonding can be identified by comparing with difference spectra associated with hydrogen bonding to methanol (ε = 33)[44] (Supporting Information, Figure S5). These bands are observed at (−) 859 (W17), (−) 1012 (W16), (−) 1345 (W7), and (−) 1616 (W1) cm^{-1} (Supporting Information, Figure S5B, for example). The band most sensitive to dielectric changes, with ~40 cm^{-1} shifts, is the W17 band. For example, a shift from 896 to 859 cm^{-1} is observed when the cyclohexane (ε = 2.0) is compared to the chloroform (ε = 4.8) difference spectrum (Supporting Information, Figure S5B, C). In agreement with these results, increasing frequency for the W17 mode has been shown previously to be correlated with a weakening of tryptophan hydrogen bonding and a lower dielectric constant.[45−48] In the model 3-methylindole data, a positive band at 1549−1551 cm^{-1} is also associated with hydrogen-bonding changes in the low dielectric solvent cyclohexane (Figure 5B and Supporting Information, Figure S5C,D, blue), but not in the higher dielectric solvent, chloroform (Supporting Information, Figure S5B).

Comparison of these data to the Apo-β2 − Met-β2 spectrum (Figure 5A) identifies 3-methylindole spectral changes associated with hydrogen-bonding changes. For example, negative bands at 880, 1010, and 1351 cm^{-1} (Figure 5A and S5, dashed lines) and a positive band at 1560 cm^{-1} (Figure 5A, blue) in the

β2 difference spectrum correspond to features marking a change in hydrogen bonding in a low dielectric environment (Figure 5B and Supporting Information, Figure S5B−D). These data imply that the perturbed β2 tryptophan is buried and increases in hydrogen bonding when the metal cluster is removed.

A negative band at 1542 cm^{-1} appears in the β2 spectrum (Figure 5A, green) but not in the model 3-methylindole spectra (Figure 5B and Supporting Information, Figure S5). The closest corresponding band in the model 3-methylindole spectra is observed at (−) 1558−1562 cm^{-1}. The frequency of this band is minimally sensitive (4 cm^{-1}) to dielectric (compare Supporting Information, Figure S5B−D), and therefore, a dielectric change alone is not consistent with the ∼20 cm^{-1} downshift observed in the β2 spectrum. This W3 band at ∼1550 cm^{-1} is a known conformation marker for tryptophan.[47] The frequency of this band is affected by the torsion angle, $\chi^{2,1}$, about the $C_2{=}C_3{-}C_\beta{-}C_\alpha$ linkage. The correlation $\upsilon(W3) = 1542 + 6.7(\cos 3 \times |\chi^{2,1}| + 1)^{1/2}$ between the frequency of the W3 band and tryptophan dihedral angle has been proposed.[49] This correlation, which neglects effects of hydrogen bonding, predicts that a frequency of 1542 cm^{-1} is associated with a dihedral angle of ±60°. We attribute the unique band at 1542 cm^{-1} to conformational selection in the protein, which is not modeled in the 3-methyl indole solution spectrum. To explain our data, this conformational selection must be unique to the Met-β2 state, implying that a conformational rearrangement occurs with metal cluster removal.

There are 14 tryptophan residues in the β2 dimer (7 residues in each monomer).[41] The total intensity of the W16 band (∼1010 cm^{-1}) in Figure 3 is approximately 17 000 counts. This band can be used as an internal intensity marker, because its frequency is relatively insensitive to dielectric changes (Supporting Information, Figure S5B−D). The intensity of the negative 1010 cm^{-1} W16 band in the Apo-β2 − Met-β2 difference is approximately 700 counts. This analysis suggests that at least one tryptophan residue is perturbed by dielectric/hydrogen bonding and by dihedral angle changes, when the Apo-β2 and Met-β2 states are compared.

A study of the p^2H dependence on the difference spectra was carried out over the p^2H range 6.5−9.0 (Supporting Information, Figures S6 and S7). The p^2H range was limited by the stability of the diiron cluster.[7] A subset of tryptophan vibrational modes, W17 (880 cm^{-1}), W7 (1353 cm^{-1}), and W16 (1013 cm^{-1}), exhibited an intensity change with p^2H titration. A previous X-ray crystallographic study of pH-induced structural changes was conducted for the diferrous form of the β subunit at pH 5.0 and 7.3. While monomer B exhibited no significant changes, alterations in the ligand environment of the iron cluster were observed in monomer A.[50] The observation of pH-induced changes is consistent with the assignment of these bands to one or more tryptophan residues near the metal cluster, which are perturbed by conformational and hydrogen-bonding rearrangements.

To summarize, our results suggest that at least one tryptophan, close to the metal cluster, protected from exchange, and in a low dielectric environment, is perturbed by a hydrogen-bonding and conformational rearrangement, when the iron cluster is removed.

Spectral Changes Induced by Iron Cluster Removal, Relative to a Met-β2 Sample: Perturbations of Tyrosine. The spectrum in Figure 5A cannot be completely explained by tryptophan contributions. Comparison to model compound data suggests that spectral alterations from tyrosine residues are also observed. For example, bands at 1170 (−) and 1185 (+) in Figure 4B are clearly assignable to tyrosine (Supporting Information, Table S1). In addition, the negative bands at 1611, 1593, 1204, and 846 cm^{-1} may contain contributions from tyrosine. Supporting the assignment to tyrosine, the negative 1593 cm^{-1} Y8b mode (Figure 4B) shifts to 1581 cm^{-1} with ^2H-exchange (Figure 4C). This is characteristic for the Y8b band of the protonated phenolic side chain (Supporting Information, Figure S1A and inset).[51]

The intensity of the Y9a tyrosine feature at 1170 cm^{-1} (Figure 4B) corresponds to approximately 7% of the total tyrosine signal observed in control β2 (Figure 3). Because dimeric β2 contains 32 tyrosine residues,[41] this result suggests that two tyrosine residues contribute to the tyrosine signal changes observed in Figure 4B. These two tyrosines may be Y122 (in chain A and B), which are located within 6 Å of the iron cluster. The 1204 cm^{-1} frequency for tyrosine Y7a in Figure 4B is different from the 1199 cm^{-1} frequency observed in the control − Met-β2 spectrum (Figure 4A). This may be due to an overlapping spectral perturbation from the positive band at 1185 cm^{-1} in Figure 4B. Observation of a tyrosine Y7a band at 1204 cm^{-1} supports the conclusion that the perturbed tyrosine residue(s) is hydrogen bonded in the Met-β2 state.[12] The 1170 cm^{-1} band is sensitive to conformation and the 1204 cm^{-1} band is sensitive to hydrogen bonding,[39] so we attribute this spectral contribution to a structural rearrangement of two tyrosine residues. From comparison of the crystal structures of the Met and Apo forms (Figure 1), a decrease in the Y122-D84 distance is observed, consistent with a hydrogen-bonding change.

UVRR Intensities. The UVRR difference spectra of β2 (Figures 4B,C) are dominated by negative bands. Our model compound spectra, studying the effect of hydrogen bonding and dielectric constant on 3-methylindole, mimic this effect. In previous work, it was concluded that changes in hydrogen bonding alter the intensity and λ_{max} of optical transitions in 3-methylindole and tryptophan methyl ester.[45,52] Hydrogen-bonding-induced shifts of the absorption spectra of tyrosine and phenol are also expected.[52−55] For 3-methylindole, hydrogen bonding resulted in a decrease in the Raman cross section from 250 to 270 nm but an overall increase in observed Raman intensities at 229 nm.[45] In our work, we have scaled the data for overall changes in Raman cross section through our baseline subtraction method. However, the fact that our β2 spectra are dominated by negative bands could still be consistent with an optical absorption shift when the Apo-β2 and Met-β2 states are compared. Another possibility is that changes in metal content lead to alterations in resonance enhancement mechanism, which could change Raman intensities.[27,38,56]

Spectral Changes Induced by Iron Cluster Removal, Relative to a Met-β2 Sample: Perturbations of Histidine. With ^2H exchange of protonated histidine in solution, the $\upsilon(N\tau{-}C_2{-}N\pi)$ symmetric stretch intensifies and shifts to 1408 cm^{-1} (Supporting Information, Figure S4A, green and refs 29, 57, 58). Figure 4D,E are difference spectra, associated with the protonation of model histidine *in vitro*. A 1407 cm^{-1} band dominates the difference spectrum acquired in ^2H_2O buffer (Figure 4E) but is not observed in ^1H_2O buffer (Figure 4D). Similarly, a 1405 cm^{-1} band is observed in the ^2H exchanged Apo-β2 − Met-β2 difference spectrum (Figure 4C and Supporting Information, Table S1) but not in ^1H_2O buffer (Figure 4B). This observation provides

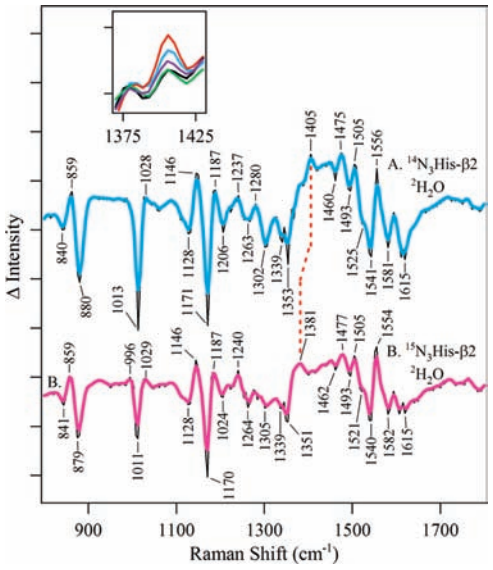

Figure 6. UVRR difference spectrum of *E. coli* β2 samples, showing the effect of $^{15}N_3$-histidine labeling. The data are natural abundance Apo-β2 − Met-β2 in 5 mM HEPES-NaOL, p^{2}H 7.6 (A) and ^{15}N-histidine labeled Apo-β2 − Met-β2 in 5 mM HEPES-NaOL, p^{2}H 7.6 (B). The spectrum in part A is reproduced from Figure 4C, for comparison. The light blue and purple lines correspond to a three adjacent point smoothing fit to the raw (thin black line) data.[71] The spectra are averages of data obtained from 10 separate samples. In the inset, the 1405 cm^{-1} band is shown as a function of p^{2}H. The data are natural abundance Apo-β2 − Met-β2 in 5 mM MES-NaOL [2-(*N*-morpholino)ethanesulfonic acid], p^{2}H 6.5 (red); 5 mM Tris-^{2}HCl, p^{2}H 7.6 (light blue); 5 mM Tris-^{2}HCl, p^{2}H 8.0 (purple); 5 mM Tris-^{2}HCl, p^{2}H 8.5 (green); and 5 mM Tris-^{2}HCl, p^{2}H 9.0 (black). See also Supporting Information, Figures S6 and S7. The protein concentrations were 50 μM. The *y*-axis tick marks represent 5 × 10^2 intensity units.

evidence for protonation of histidine with metal cluster removal from the β2 subunit. The histidine has an elevated p*K*, because a 1405 cm^{-1} band is observed in the p^{2}H range from 6.5 to 9.0 (Figure 6, inset, and Figure S6, Supporting Information).

To confirm this interpretation, the β2 subunit was labeled with $^{15}N_3$-histidine (Figure 6B) and compared to a natural abundance sample (Figure 6A). As shown in Figure S4D of the Supporting Information for histidine in vitro, ^{15}N labeling of histidine results in a 26 cm^{-1} downshift of the 1408 cm^{-1} band. This downshift is expected from previous studies.[59] Figure 6A,B shows a similar downshift [1405 (+) to 1381 (+) cm^{-1}] in the $^{15}N_3$-histidine-labeled Apo-β2 − Met-β2 spectrum. We conclude that histidine ligands protonate when the iron is removed from the β2 subunit. The other vibrational bands of histidine are not expected to be observed, because these bands are not as intense as the 1408 cm^{-1} band and are less sensitive to $^{15}N_3$ labeling (Supporting Information, Figure S4D). The intensity of the 1405 cm^{-1} band cannot be used to predict the number of histidine residues perturbed in the difference spectrum. This is because a Raman band from histidine is not clearly identifiable before subtraction (Figure 3), due to the low Raman cross section of this spectral feature. Normalization for the intensity of Raman scattering is necessary for a quantitative comparison.

DISCUSSION

Structure of the Metal-Free β2 Subunit. In RNR, formation of the iron cluster occurs by binding ferrous ions to a folded protein, followed by metal oxidation. In the ferric form, the +6 charge on the two iron ions is compensated by two negative charges provided by a bridging O^{2-} and by the ligating, negatively charged Asp84, Glu115, Glu204, and Glu238 side chains. Structures of the diferric (Met-β2, Figure 1A), diferrous (Red-β2), and metal free (Apo-β2, Figure 1B) forms of the β2 subunit are available.[9−12] The structure of the metal-free β2 subunit shows that the carboxylates at the iron site change their rotameric conformation when the iron is removed.[9] Changes in the position and content of bound water molecules are also observed. p*K* shifts may occur, and low-barrier hydrogen bonds between carboxylate groups may form. These changes may compensate for destabilizing electrostatic effects.[60] While protonation state could not be directly resolved at the available structural resolution, it was proposed that histidine residues protonate when the iron is removed from the β2 subunit.[60]

Protein Conformational Changes Are Expected To Accompany Diiron Cluster Assembly. Reaction of Apo-β2 with Fe^{2+}, O_2, and excess reductant generates 1.2 tyrosyl radicals per β2 subunit and a Fe^{2+}/Y122• stoichiometry of 3.3.[61] The metal cluster binding site is 10 Å from the surface, and there is no obvious channel through which metal can access the binding site.[9] Each β monomer contains two inequivalent iron binding sites, Fe_A and Fe_B, which have a 5-fold difference in metal affinity.[17,62] Intermediates in the assembly process can be detected (reviewed in ref 8). When reducing equivalents are abundant, an intermediate, X, accumulates with a rate constant of 8 s^{-1} and decays with the formation of the diferric cluster (0.8 s^{-1}).[15] X generates the tyrosyl radical by oxidation of Y122.[6,15,61,63−65] When reducing equivalents are limiting, a transient signal from a W48 tryptophan cation radical can be detected.[66,67] W48H$^+$• can also oxidize Y122 to generate the tyrosyl radical.[66]

Because the rate constant for formation of X is independent of the concentrations of reactants, it was proposed that the 8 s^{-1} first-order rate constant reflects a protein conformational change.[15] Subsequent work has shown that binding of metal to the high affinity Fe_B site causes a global conformational change, which inhibits iron binding to the other β protomer.[17,68] Filling the Fe_B site also has been reported to inhibit metal binding to the Fe_A site[17] through an allosteric effect.

UVRR Spectroscopy Identifies Protein Conformational Changes. In this work, we describe structural changes that are linked to the assembly of the iron cluster and to the reduction of the tyrosyl radical in RNR. Spectral contributions from tyrosine, tryptophan, and histidine were resonantly enhanced using a UV Raman probe beam. The vibrational frequencies and intensities of these amino acids are structural markers in proteins.[19,69,70] UVRR has previously been applied to monitor electron transfer reactions,[71] protonation changes,[72,73] folding,[74] allosteric conformational changes,[70] and dynamics.[75,76] Contributions from carboxylic acid side chains are not detectable with UV probe wavelengths (data not shown).

Reduction of Y122. The control − Met-β2 spectrum reflects redox changes to Y122. In particular, we observe the diagnostic CO (Y7a, 1499 cm^{-1}) and ring stretching (Y8a, 1556 cm^{-1}) vibrations of the tyrosyl radical, Y122•, and several normal modes, at 1170, 1199, and 1608 cm^{-1}, arising from the reduced

tyrosine, Y122. The upshift of the CO vibration to 1499 cm^{-1} from the ~1250 cm^{-1} CO frequency expected in singlet tyrosine is caused by the delocalization of spin density onto the phenolic oxygen.[30] Recently, FT-IR spectroscopy has detected the same 1499 cm^{-1} CO band and has shown that redox changes to Y122 result in perturbations of the amide bond.[13] In RNR, Y122 oxidation causes a loss of hydrogen-bond communication to the diiron cluster and rotation of the aromatic ring.[12] The trigger for the observed conformational changes may be the change in hydrogen-bonding interactions between Y122•/Y122 and D84[12] or the electrostatic changes induced by Y122• reduction.[77] Our results show that these conformational changes have little effect on the other aromatic amino acid residues in the vicinity of Y122.

Deprotonation of Histidine Is Associated with Assembly of the Metal Cluster. Clustering of negatively charged amino acids in the interior of proteins is unusual. Therefore, it has been proposed that protonation of histidines compensates for charge differences induced by loss of iron.[60] Alternatively, the polar nature of the metal binding site, which is located 10 Å from the surface of the protein, might lead to dipolar relaxation.

Our UVRR Raman data provide evidence for histidinium in the Apo-β2 subunit, even at slightly alkaline pL (i.e., p^2H 7.6). The presence of a protonated histidine at pL 7.6 suggests an environmental influence, which increases the pK of the histidine side chain. Our pL titration study supports this conclusion. An increase in histidine pK could be due to the negative charges on the carboxylate ligands, which will tend to stabilize the protonated form of the imidazole side chains. Of the eight histidine residues in the β subunit, the only histidine residues within 11 Å of the cluster are the ligating histidines, H118 and H241 (Figure 1). Therefore, we suggest that the charge states of H118 and H241 change with metal cluster assembly.

Tryptophan Structural Changes Are Associated with Assembly of the Metal Cluster. Our UVRR data provide evidence for a perturbation of tryptophan with metal cluster removal. Alterations both in the frequency and the intensity of vibrational bands are observed. The literature establishes that changes in the Raman intensities or frequency shifts correlate with alterations in the tryptophan environment.[45,78,79] These redox-linked structural changes may underlie the allosteric effects described above.[17,68]

In this paper, we present model compound spectra obtained from 3-methylindole in different solvents. These difference spectra were constructed by subtraction of data acquired in non-hydrogen-bonding and hydrogen-bonding environments. Comparison of the 3-methylindole and protein spectra suggests that the perturbed tryptophan(s) in β2 are exposed to a more hydrogen bonding environment in Apo-β2. The data also suggest that the tryptophans reorient with removal of the iron cluster. Our studies imply that the affected tryptophan is near the active site and protected from solvent exchange.

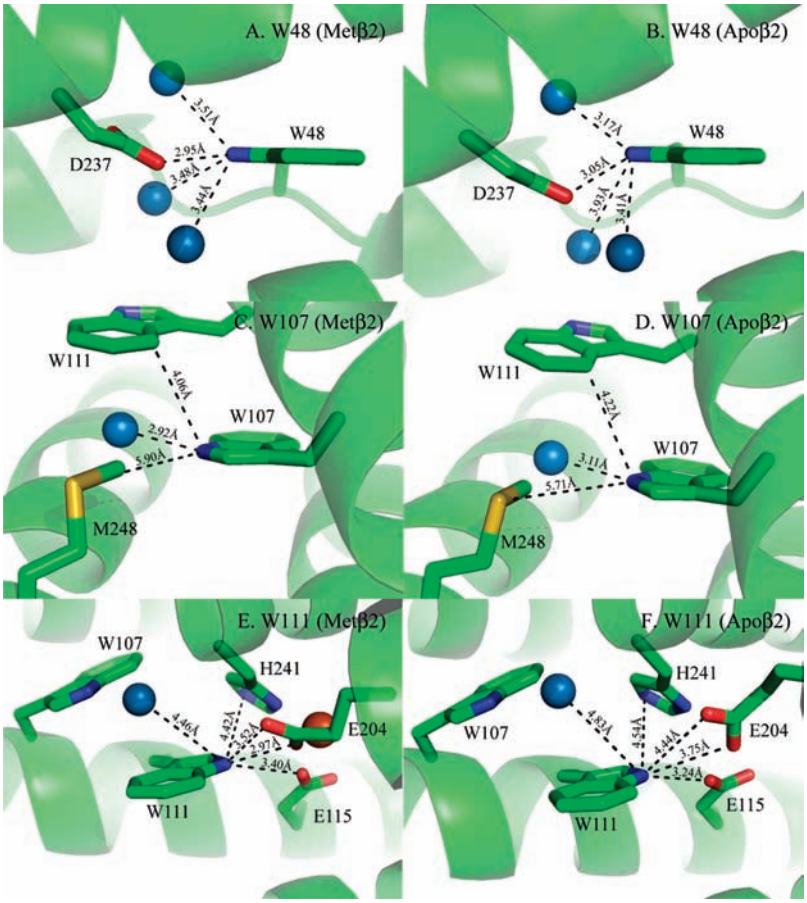

Figure 7. Environments of three tryptophan residues, W48 (A and B), W107 (C and D), and W111 (E and F), in the β2 subunit. The Met-β2 (A, C, E) and Apo-β2 (B, D, F) X-ray structures illustrate the changes associated with iron removal.[9,12,60] The spheres in blue represent the oxygen atom of modeled water molecules, and the sphere in orange represents an iron atom of the diiron cluster. Amino acid residues and water molecules within 5 Å of the tryptophan indole nitrogen are shown, and the corresponding distances are labeled in Å (PDB coordinates were graciously provided by H. Eklund).

dx.doi.org/10.1021/ja107918g |*J. Am. Chem. Soc.* 2011, 133, 6978–6988

There are three tryptophan residues, W111, W107, and W48, within 11 Å of the iron cluster (Figure 1). W48, which has been linked to Y122• formation and substrate-induced PCET, is ~9 Å from the nearest iron atom. W48 participates in a potential hydrogen-bonding network with one of the histidine ligands (Figure 1) and forms a transient tryptophan cation radical under some conditions.[66,67] W48 exchanges protons with Asp237, adjacent to Glu238, potentially to mediate PCET directionality.[5,80] W107 is 9 Å and W111 is 4 Å from the iron cluster; these tryptophans are not predicted to be in a hydrogen-bonding network with the iron cluster (Figure 1).

Figure 7 shows a prediction of hydrogen-bonding interactions with each of these three tryptophans, based on analysis of the Met-β2 (A, C, and E) and Apo-β2 (B, D, and F) structures. The expected position of bound water molecules is shown in the blue spheres. W48 is predicted to hydrogen bond to water molecules and D237 in the Met state, and the hydrogen bonds exhibit only small changes in the Apo state. W107 is predicted to interact with a nearby water molecule in both states. W111 is hydrogen bonded to E115 in the Met form of the protein. E204 changes conformation with iron cluster removal and has a new potential electrostatic interaction with W111. On the basis of these structures, W111 is a likely contributor to the Apo-β2 − Met-β2 UVRR difference spectra.

The dihedral angles of W48, W107, and W111 in the Met-β2 (chain A) form of the β2 subunit are −78°, −120°, and 18°, respectively.[12] In chain B, the angles are −80°, −121°, and 21°. In the Apo-β2 state, these angles are −88/−79°, −123/−124°, 14/10° (chain A/chain B). The 1542 cm^{-1} frequency of the perturbed tryptophan predicts a conformation of ±60° in the Met-β2 state and a conformational change when the Apo-β2 state is formed. Given these values for the dihedral angles, the negative 1542 cm^{-1} peak in Figure 4B would be attributed to W48 in Met-β2. However, the W3 band is also sensitive to hydrogen bonding,[45] complicating this analysis. To conclude, our UVRR data, which probe solution dynamics, are consistent with an electrostatic and structural change either in W48 or W111.

A Tyrosine Conformational Change Is Associated with Assembly of the Metal Cluster. Perturbations of bands at 1170 (−) and 1185 (+) cm^{-1} are observed in the Apo-β2 − Met-β2 difference spectrum and are diagnostic of structural perturbations to tyrosine. There are three tyrosine residues within 11 Å of the iron cluster, redox active Y122, Y209, and Y157 (Figure 1). Y122 has a hydrogen-bonding interaction with Asp84, which is in turn within hydrogen-bonding distance of ligating His118 (Figure 1).[12] The high-resolution structure of Met-β2 supports a weak hydrogen bond between Tyr122 and Asp84[12] (but see ref 11). Iron removal induces a shortening of the distance between the two residues from 3.3 to 2.7 Å.[9] This change suggests a strengthening of the hydrogen bond between the Y122 and D84 residues in the Apo-β2 form of the β2 subunit. However, the Y9a frequency is influenced mainly by the Y−OH configuration,[39] so we attribute the spectral change in tyrosine bands to a conformational or hydrogen bonding alteration at Y122. Redox-driven changes in conformation have been reported for Y122 previously.[12,13]

Comparison of Metal Cluster Assembly in RNR with Other Diiron Nonheme Proteins. Diferric nonheme proteins, such as RNR, soluble methane monooxygenase hydroxylase (MMOH), and stearoyl acyl carrier protein Δ^9-desaturase (Δ9D), catalyze a diverse range of reactions.[81−83] Although the functions of these enzymes differ, they each have a similar diiron center with coordination from two histidine and four carboxylate residues.[84] In RNR, MMOH, and Δ9D, the iron center is buried in the protein, and assembly of the cluster could disrupt the conformation of the protein through electrostatic effects. X-ray structures of the metal-free MMOH[85] and Δ9D[86] have been reported. The global changes observed in the structure of the metal-free proteins are relatively minor, when compared to their respective holoenzymes. Some of the normally coordinating carboxylates are disordered, suggesting a lack of charge compensation. As opposed to the carboxylate ligands, the histidine ligands in MMOH are highly ordered, and protonation of the histidines was considered unlikely.[85] As with the metal-free MMOH structure, the protonation state of histidine in Apo-Δ9D was not clear.[86] Overall, the metal-free forms of these nonheme diiron proteins exhibit stable structures, even in the absence of charges provided by the metal clusters. Thus, all three proteins have evolved to accommodate assembly of the metal cluster in a folded form of the protein.

Summary. The conformational perturbations of tryptophan, tyrosine, and histidine residues, measured here, are associated with assembly of the iron cluster. These changes are caused by alterations in hydrogen bonding and conformation. Such conformational plasticity is likely to play a role in facilitating the assembly of the metal cluster, and these structural changes are likely to contribute to the conformational change, which has previously been proposed[15] to accompany metal binding and oxidation.

■ ASSOCIATED CONTENT

Supporting Information. UVRR spectra of tyrosine, phenylalanine, tryptophan, histidine, and 3-methylindole; a table of assignments; and a p^2H study of the β2 subunit. This material is available free of charge via the Internet at http://pubs.acs.org.

■ AUTHOR INFORMATION

Corresponding Author
bridgette.barry@chemistry,gatech.edu

Present Addresses
[†]Dalian National Laboratory for Clean Energy, Dalian Institute of Chemical Physics, Chinese Academy of Science, Dalian 116023, China

■ ACKNOWLEDGMENT

The authors thank Prof. JoAnne Stubbe and Ellen Minnihan for helpful discussions and for providing protocols for metal-free β2 production. The authors are grateful to Prof. John Markeley and Dr. Fariba Assadi-Porter for providing AW608Thr cells and to Prof. H. Eklund and Prof. P. Nordlund for sharing the coordinates of the Apo-β2 structure. This project was supported by Award Number R01GM043273 from the National Institute of General Medical Sciences and the National Eye Institute.

■ REFERENCES

(1) Thelander, L.; Reichard, P. *Annu. Rev. Biochem.* **1979**, *48*, 133–158.
(2) Stubbe, J. *J. Biol. Chem.* **1990**, *265*, 5329–5332.
(3) Stubbe, J.; Riggs-Gelasco, P. *Trends Biochem. Sci.* **1998**, *23*, 438–443.

(4) Uhlin, U.; Eklund, H. *Nature* **1994**, *370*, 533–539.
(5) Stubbe, J.; Nocera, D. G.; Yee, C. S.; Chang, M. C. *Chem. Rev.* **2003**, *103*, 2167–2201.
(6) Bollinger, J. M., Jr.; Edmondson, D. E.; Huynh, B. H.; Filley, J.; Norton, J. R.; Stubbe, J. *Science* **1991**, *253*, 292–298.
(7) Atkin, C. L.; Thelander, L.; Reichard, P.; Lang, G. *J. Biol. Chem.* **1973**, *248*, 7464–7472.
(8) Stubbe, J. *Curr. Opin. Chem. Biol.* **2003**, *7*, 183–188.
(9) Åberg, A.; Nordlund, P.; Eklund, H. *Nature* **1993**, *361*, 276–278.
(10) Logan, D. T.; Su, X.-D.; Åberg, A.; Regnström, K.; Hajdu, J.; Eklund, H.; Nordlund, P. *Structure* **1996**, *4*, 1053–1064.
(11) Nordlund, P.; Sjöberg, B.-M.; Eklund, H. *Nature* **1990**, *345*, 593–598.
(12) Högbom, M.; Galander, M.; Andersson, M.; Kolberg, M.; Hofbauer, W.; Lassmann, G.; Nordlund, P.; Lendzian, F. *Proc. Natl. Acad. Sci. U. S. A.* **2003**, *100*, 3209–3214.
(13) Offenbacher, A. R.; Vassiliev, I. R.; Seyedsayamdost, M. R.; Stubbe, J.; Barry, B. A. *J. Am. Chem. Soc.* **2009**, *131*, 7496–7497.
(14) Ge, J.; Yu, G.; Ator, M. A.; Stubbe, J. *Biochemistry* **2003**, *42*, 10071–10083.
(15) Tong, W. H.; Chen, S.; Lloyd, S. G.; Edmondson, D. E.; Huynh, B. H.; Stubbe, J. *J. Am. Chem. Soc.* **1996**, *118*, 2107–2108.
(16) Umback, N. J.; Norton, J. R. *Biochemistry* **2002**, *41*, 3984–3990.
(17) Pierce, B. S.; Hendrich, M. P. *J. Am. Chem. Soc.* **2005**, *127*, 3613–3623.
(18) Nagai, M.; Wajcman, H.; Lahary, A.; Nakatsukasa, T.; Nagatomo, S.; Kitagawa, T. *Biochemistry* **1999**, *38*, 1243–1251.
(19) Takeuchi, H. *Biopolymers* **2003**, *72*, 305–317.
(20) Seyedsayamdost, M. R. Thesis, Massachusettes Institute of Technology, 2008.
(21) Jenson, D. L.; Barry, B. A. *J. Am. Chem. Soc.* **2009**, *131*, 10567–10573.
(22) Xia, B.; Cheng, H.; Skjeldal, L.; Coghlan, V. M.; Vickery, L. E.; Markley, J. L. *Biochemistry* **1995**, *34*, 180–187.
(23) Xia, B.; Pikus, J. D.; Xia, W.; McClay, K.; Steffan, R. J.; Chae, Y. K.; Westler, W. M.; Markley, J. L.; Fox, B. G. *Biochemistry* **1999**, *38*, 727–739.
(24) Chen, J.; Barry, B. A. *Photochem. Photobiol.* **2008**, *84*, 815–818.
(25) Garbett, K.; Darnall, D. W.; Klotz, I. M.; Williams, R. J. *Arch. Biochem. Biophys.* **1969**, *135*, 419–434.
(26) Petersson, L.; Gräslund, A.; Ehrenberg, A.; Sjöberg, B. M.; Reichard, P. *J. Biol. Chem.* **1980**, *255*, 6706–6712.
(27) Rava, R. P.; Spiro, T. G. *J. Phys. Chem.* **1985**, *89*, 1856–1861.
(28) Sweeny, J. A.; Asher, S. A. *J. Phys. Chem.* **1990**, *94*, 4784–4791.
(29) Caswell, D. S.; Spiro, T. G. *J. Am. Chem. Soc.* **1986**, *108*, 6470–6477.
(30) Tripathi, G. N.; Schuler, R. H. *J. Chem. Phys.* **1984**, *81*, 113–121.
(31) Johnson, C. R.; Ludwig, M.; Asher, S. A. *J. Am. Chem. Soc.* **1986**, *108*, 905–912.
(32) Ayala, I.; Range, K.; York, D.; Barry, B. A. *J. Am. Chem. Soc.* **2002**, *124*, 5496–5505.
(33) Bent, D. V.; Hayon, E. *J. Am. Chem. Soc.* **1975**, *97*, 2599–2606.
(34) Range, K.; Ayala, I.; York, D.; Barry, B. A. *J. Phys. Chem. B* **2006**, *110*, 10970–10981.
(35) Backes, G.; Sahlin, M.; Sjöberg, B.-M.; Loehr, T. M.; Sanders-Loehr, J. *Biochemistry* **1989**, *28*, 1923–1929.
(36) Kim, S.; Barry, B. A. *Biochemistry* **1998**, *37*, 13882–13892.
(37) Ayala, I.; Kim, S.; Barry, B. A. *Biophys. J.* **1999**, *77*, 2137–2144.
(38) Fodor, S. P. A.; Copeland, R. A.; Grygon, C. A.; Spiro, T. G. *J. Am. Chem. Soc.* **1989**, *111*, 5509–5518.
(39) Takeuchi, H.; Watanabe, N.; Satoh, Y.; Harada, I. *J. Raman Spectrosc.* **1989**, *20*, 233–237.
(40) Suydam, I. T.; Boxer, S. G. *Biochemistry* **2003**, *42*, 12050–12055.
(41) Carlson, J.; Fuchs, J. A.; Messing, J. *Proc. Natl. Acad. Sci. U. S. A.* **1984**, *81*, 4294–4297.
(42) Takeuchi, H.; Harada, I. *Spectrochim. Acta, Part A* **1986**, *42*, 1069–1078.
(43) Liu, G. Y.; Grygon, C. A.; Spiro, T. G. *Biochemistry* **1989**, *28*, 5046–5050.
(44) Lide, D. R. *CRC Handbook of Chemistry and Physics*, 85th ed.; CRC Press: Boca Ranton, FL, 2004; pp 8−141.
(45) Matsuno, M.; Takeuchi, H. *Bull. Chem. Soc. Jpn.* **1998**, *71*, 851–857.
(46) Miura, T.; Takeuchi, H.; Harada, I. *Biochemistry* **1988**, *27*, 88–94.
(47) Miura, T.; Takeuchi, H.; Harada, I. *J. Raman Spectrosc.* **1989**, *20*, 667–671.
(48) Kochendoerfer, G. G.; Kaminaka, S.; Mathies, R. A. *Biochemistry* **1997**, *36*, 13153–13159.
(49) Maruyama, T.; Takeuchi, H. *Biochemistry* **1997**, *36*, 10993–11001.
(50) Voegtli, W. C.; Sommerhalter, M.; Saleh, L.; Baldwin, J.; Bollinger, J. M., Jr.; Rosenzweig, A. C. *J. Am. Chem. Soc.* **2003**, *125*, 15822–15830.
(51) Copeland, R. A.; Spiro, T. G. *Biochemistry* **1985**, *24*, 4960–4968.
(52) Bailey, J. E.; Beaven, G. H.; Chignell, D. A.; Gratzer, W. B. *Eur. J. Biochem.* **1968**, *7*, 8–14.
(53) Baba, H.; Suzuki, S. *J. Chem. Phys.* **1961**, *35*, 1118–1127.
(54) Donovan, J. W. *J. Biol. Chem.* **1969**, *244*, 1961–1967.
(55) Rothschild, K. J.; Roepe, P.; Ahl, P. L.; Earnest, T. N.; Bogomolni, R. A.; Das Gupta, S. K.; Mulliken, C. M.; Herzfeld, J. *Proc. Natl. Acad. Sci. U. S. A.* **1986**, *83*, 347–351.
(56) Rava, R. P.; Spiro, T. G. *J. Am. Chem. Soc.* **1984**, *106*, 4062–4064.
(57) Tasumi, M.; Harada, I.; Takamatsu, T.; Takahashi, S. *J. Raman Spectrosc.* **1982**, *12*, 149–151.
(58) Gregoriou, V. G.; Jayaraman, V.; Hu, X.; Spiro, T. G. *Biochemistry* **1995**, *34*, 6876–6882.
(59) Zhao, X.; Chen, R.; Deng, Q.; Mabrouk, P. A.; Spiro, T. G. *Isr. J. Chem.* **2000**, *40*, 15–20.
(60) Andersson, M. E.; Högbom, M.; Rinaldo-Matthis, A.; Blodig, W.; Liang, Y.; Persson, B.-O.; Sjöberg, B.-M.; Su, X.-D.; Nordlund, P. *Biochemistry* **2004**, *43*, 7966–7972.
(61) Bollinger, J. M., Jr.; Tong, W. H.; Ravi, N.; Huynh, B. H.; Edmondson, D. E.; Stubbe, J. *J. Am. Chem. Soc.* **1994**, *116*, 8015–8023.
(62) Bollinger, J. M., Jr.; Chen, S.; Parkin, S. E.; Mangravite, L. M.; Ley, B. A.; Edmondson, D. E.; Huynh, B. H. *J. Am. Chem. Soc.* **1997**, *119*, 5976–5977.
(63) Burdi, D.; Sturgeon, B. E.; Tong, W. H.; Stubbe, J.; Hoffman, B. M. *J. Am. Chem. Soc.* **1996**, *118*, 281–282.
(64) Sturgeon, B. E.; Burdi, D.; Chen, S.; Huynh, B.-H.; Edmondson, D. E.; Stubbe, J.; Hoffman, B. M. *J. Am. Chem. Soc.* **1996**, *118*, 7551–7557.
(65) Willems, J.-P.; Lee, H.-I.; Burdi, D.; Doan, P. E.; Stubbe, J.; Hoffman, B. M. *J. Am. Chem. Soc.* **1997**, *119*, 9816–9824.
(66) Baldwin, J.; Krebs, C.; Ley, B. A.; Edmondson, D. E.; Huynh, B. H.; Bollinger, J. M., Jr. *J. Am. Chem. Soc.* **2000**, *122*, 12195–12206.
(67) Krebs, C.; Chen, S.; Baldwin, J.; Ley, B. A.; Patel, U.; Edmondson, D. E.; Huynh, B. H.; Bollinger, J. M., Jr. *J. Am. Chem. Soc.* **2000**, *122*, 12207–12219.
(68) Pierce, B. S.; Elgren, T. E.; Hendrich, M. P. *J. Am. Chem. Soc.* **2003**, *125*, 8748–8759.
(69) Austin, J. C.; Jordan, T.; Spiro, T. G. In *Biomolecular Spectroscopy*; Clark, R. J. H., Hester, R. E., Eds.; John Wiley & Sons Ltd.: New York, 1993; pp 55−125.
(70) Hu, X.; Spiro, T. G. *Biochemistry* **1997**, *36*, 15701–15712.
(71) Chen, J.; Bender, S. L.; Keough, J. M.; Barry, B. A. *J. Phys. Chem. B* **2009**, *113*, 11367–11370.
(72) Asher, S. A.; Larkin, P. J.; Teraoka, J. *Biochemistry* **1991**, *30*, 5944–5954.
(73) Wu, Q.; Li, F.; Wang, W.; Hecht, M. H.; Spiro, T. G. *J. Inorg. Biochem.* **2002**, *88*, 381–387.
(74) Sanchez, K. M.; Neary, T. J.; Kim, J. E. *J. Phys. Chem. B* **2008**, *112*, 9507–9511.
(75) Balakrishnan, G.; Weeks, C. L.; Ibrahim, M.; Soldatova, A. V.; Spiro, T. G. *Curr. Opin. Struct. Biol.* **2008**, *18*, 623–629.

(76) Zhu, L. Y.; Kim, J.; Mathies, R. A. *J. Raman Spectrosc.* **1999**, *30*, 777–783.
(77) Sibert, R.; Josowicz, M.; Porcelli, F.; Veglia, G.; Range, K.; Barry, B. A. *J. Am. Chem. Soc.* **2007**, *129*, 4393–4400.
(78) Takeuchi, H.; Matsuno, M.; Overman, S. A.; Thomas, G. J., Jr. *J. Am. Chem. Soc.* **1996**, *118*, 3498–3507.
(79) Okada, A.; Miura, T.; Takeuchi, H. *Biochemistry* **2001**, *40*, 6053–6060.
(80) Reece, S. Y.; Hodgkiss, J. M.; Stubbe, J.; Nocera, D. G. *Philos. Trans. R. Soc. B* **2006**, *361*, 1351–1364.
(81) Lipscomb, J. D. *Annu. Rev. Microbiol.* **1994**, *48*, 371–399.
(82) Baik, M.-H.; Newcomb, M.; Friesner, R. A.; Lippard, S. J. *Chem. Rev.* **2003**, *103*, 2385–2419.
(83) Fox, B. G.; Lyle, K. S.; Rogge, C. E. *Acc. Chem. Res.* **2004**, *37*, 421–429.
(84) Solomon, E. I.; Brunold, T. C.; Davis, M. I.; Kemsley, J. N.; Lee, S.-K.; Lehnert, N.; Neese, F.; Skulan, A. J.; Yang, Y.-S.; Zhou, J. *Chem. Rev.* **2000**, *100*, 235–350.
(85) Sazinsky, M. H.; Merkx, M.; Cadieux, E.; Tang, S.; Lippard, S. J. *Biochemistry* **2004**, *43*, 16263–16276.
(86) Moche, M.; Shanklin, J.; Ghoshal, A.; Lindqvist, Y. *J. Biol. Chem.* **2003**, *278*, 25072–25080.